

Robot Collision Avoidance based on Artificial Potential Field with Local Attractors

Matteo Melchiorre^a, Leonardo Sabatino Scimmi^b, Laura Salamina^c, Stefano Mauro^d
and Stefano Pastorelli^e

Department of Mechanical and Aerospace Engineering, Politecnico di Torino, C.so Duca degli Abruzzi 24, Turin, Italy

Keywords: Collision Avoidance, Artificial Potential Field, Local Attractors, Motion Planning.

Abstract: This paper presents a novel collision avoidance technique that allows the robot to reach a desired position by avoiding obstacles passing through preferred regions. The method combines the classical elements of the artificial potential fields in an original manner by handling local attractors and repulsors. The exact solution, which is given in a closed form, allows to sculpt a potential field so that local minima related to the local attractors are prevented and the global minimum is unperturbed. The results show the algorithm applied to mobile robot navigation and prove the capability of local attractors to influence the robot path.

1 INTRODUCTION

Collision avoidance has long been one of the most exciting challenges in robotics. It consists in finding robot commands that satisfy task and spatial constraints so that the robot reaches a desired configuration through collision-free motion.

Over the years, several techniques have been proposed (LaValle, 2006; Siciliano, Sciavicco, Villani, & Oriolo, 2009). A possible classification can be made by distinguishing *global* and *local* methods (Abhishek, Schilberg, & Arockia Doss, 2021). Global methods allow to find a collision-free path from the initial to the final pose and require prior information of the environment. They are usually based on optimization problems, roadmaps or cell decomposition. On the other hand, local methods consist of observing the proximity of the robot to change the path locally in the presence of an obstacle. Among them it is worth mentioning artificial potential field (APF), probabilistic roadmaps and bidirectional RRT.

In particular, APF has been widely investigated because it is simple to implement and has low

computational cost. For this, it performs very well in dynamic environment, where decisions on the alternative path must be taken online and a fast robot response is required.

A first formulation of APF was given by Khatib, 1986. The robot undergoes to virtual forces obtained from the negative gradient of a potential field, built considering the target as the attractor, i.e. the global minimum of the potential, and the obstacles as repulsors, i.e. confined regions with high potential. Thereafter, major efforts have been focused on the local minimum problem, which is the main drawback of this approach. The most famous examples are the superquadratic potential function proposed by Volpe & Khosla, 1990 and the navigation function introduced by Rimon & Koditschek, 1992 and extended in Filippidis & Kyriakopoulos, 2011. Other studies that have been inspired by the drawback of the artificial potential fields lead to alternative methods, like the harmonic potential functions (Connolly & Grupen, 1993), the dynamic window (Fox, Burgard, & Thrun, 1997), the collision cone (Chakravarthy & Ghose, 1998) and the attractor dynamics (Haddadin et al., 2010).

^a <https://orcid.org/0000-0002-4409-186X>

^b <https://orcid.org/0000-0002-0537-2984>

^c <https://orcid.org/0000-0002-6330-3362>

^d <https://orcid.org/0000-0001-8395-8297>

^e <https://orcid.org/0000-0001-7808-8776>

Another branch of the potential field research moved towards more practical approaches that consider robot command in terms of a velocity vector computed from the gradient (Güldner & Utkin, 1996), or directly obtained in function of the distance from the obstacle (Mauro et al., 2017; Melchiorre et al., 2021, 2019; Scimmi et al., 2018, 2019, 2021). This allows for exact tracking of gradient lines and the convergence to the goal.

In general, the gradient vector field can be coupled with additional vector terms to prevent local minima or to generate convenient paths, that is the case with tangential fields (De Medio & Oriolo, 1991) and selective attraction (Murphy, 2000). Another example is the virtual target approach, that consists of substituting the global target with a local one around the object to avoid local minima (Long, 2020; Zou & Zhu, 2003). Alternatively, the robot goal position can be temporarily moved or projected to overcome local minima (Arslan & Koditschek, 2019; Castelnovi, Sgorbissa, & Zaccaria, 2006; Paromtchik & Nassal, 1995). Other studies consider solving optimization problem to find the global minimum (Pozna, Troester, Precup, Tar, & Preitl, 2009).

Plenty of literature works studied how to solve or improve potential fields built from a single goal and multiple obstacles but there is a lack of contribute on techniques to influence trajectory selection in order to go through specific areas. This can be fundamental for robot navigation when the obstacle has preferred approaching directions. For example, socially acceptable pre-collision criteria suggest that choosing a certain side when crossing the human path can improve legibility of robot motion (Qian, Ma, Dai, & Fang, 2010). Similar aspects arise in human-robot collaboration, where controlling the robot trajectory towards predictable regions may result in a more fluent interaction (Koppenborg, Nickel, Naber, Lungfiel, & Huelke, 2017).

The importance of finding a simple and effective solution to deal with obstacles in a controlled manner motivated the authors of this paper. The original idea is to introduce local attractors in APF in order to design the trajectories with a higher precision. Few authors consider applications of potential fields with multiple attractors and repulsors. An introduction to is given in (Beard & McClain, 2003), where, the possibility to model and combine the potential fields of each element by using quadratic or exponential function is discussed. However, (Beard & McClain, 2003) is limited to introducing the concept of multiple attractors and does not distinguish the roles of the global and local attractors.

This work investigates the possibility of using local attractors to make the robot reach the final goal by avoiding obstacles and passing through attractive regions. The main aspect that distinguishes this work from the previous ones is the addition of strategical attractive points to the one related to the global minimum. In particular, the attractive points are modelled as deflections of the potential field, without being local minima.

2 POTENTIAL FIELD WITH LOCAL ATTRACTORS

In this section, the problem of artificial potential field with local attractors is formulated. The avoidance objectives are: i) to reach a desired position from a starting configuration; ii) to avoid obstacles choosing the side of local attractors; iii) to prevent local minima related to local attractors.

The approach is described in \mathbb{R}^2 . The potential field is modelled combining quadratic and exponential functions (Beard & McClain, 2003; Khatib, 1986). Thus, some considerations on the choice of the attractor intensity are given.

2.1 Problem Formulation

Consider the robot end-effector as a point in the two-dimensional cartesian space, whose task is to reach the desired position \mathbf{x}_d from a starting position \mathbf{x} . The desired position can be seen as an attractive potential field U_d , which is modelled with the quadratic function (Khatib, 1986):

$$U_d(\mathbf{x}) = \frac{1}{2}\sigma\|\mathbf{x} - \mathbf{x}_d\|^2 \quad (1)$$

where σ is a positive parameter which regulates the intensity of the quadratic function and $\mathbf{x} = [x \ y]^T$ represents the generic point in the cartesian space. In (1), it is written $U_d(\mathbf{x})$ to exploit the dependency on \mathbf{x} . In general, it is $U_d(\mathbf{x}, \mathbf{x}_d, \sigma)$ but \mathbf{x}_d is given by the task and the parameter σ is supposed to be chosen. To simplify the reading, hereafter, only the spatial variable \mathbf{x} is exploited, except where otherwise specified.

Suppose the presence of an obstacle. In general, it may have any geometry. Sometimes it is convenient to approximate objects by composing simple shapes, i.e. spheres, cylinders and planes. Other applications may need more accurate potential functions to describe the obstacles. For the discussion, only the case of the disc in two dimensions, is considered. The

reader is referred to the literature for general obstacle modelling (Khatib, 1986; Ren, McIsaac, Patel, & Peters, 2007; Rimon & Koditschek, 1992; Volpe & Khosla, 1990).

The obstacle is centred in \mathbf{x}_o , with radius R_o (Figure 1a). It produces a repulsive potential field U_o , which is modelled with the exponential function (Beard & McClain, 2003):

$$U_o(\mathbf{x}) = \beta_o e^{-\frac{\gamma_o}{2}\|\mathbf{x}-\mathbf{x}_o\|^2} \quad (2)$$

where β_o and γ_o are the positive parameters that determine the shape of the gaussian around the obstacle; in particular, β_o is the peak value, while γ_o is the exponential decay parameter. In Figure 1a, the outer circle centred in \mathbf{x}_o identifies the active region U_o^* , defined as the circle with radius R_o^* so that the gradient of U_o goes to zero outside U_o^* . The radius R_o^* can be calculated by solving $|\nabla U_o| = s_\epsilon$, where s_ϵ is a small positive value, hereafter named “zero threshold” (see Appendix A for further details):

$$R_o^* = \left[-\frac{1}{\gamma_o} W_{-1} \left(-\frac{s_\epsilon^2}{\beta_o^2 \gamma_o} \right) \right]^{1/2} \quad (3)$$

If only the goal and the obstacle are considered, the resulting total potential field U_{do} can be written as:

$$\begin{aligned} U_{do}(\mathbf{x}) &= U_d(\mathbf{x}) + U_o(\mathbf{x}) = \\ &= \frac{1}{2}\sigma\|\mathbf{x}-\mathbf{x}_d\|^2 + \beta_o e^{-\frac{\gamma_o}{2}\|\mathbf{x}-\mathbf{x}_o\|^2} \end{aligned} \quad (4)$$

The generic potential field U_{do} is shown in Figure 2a. The control law can be chosen so that the command vector has the direction of the negative gradient. In the specific case of Figure 1a, if \mathbf{x}_s , \mathbf{x}_o and \mathbf{x}_d are aligned, by following the negative gradient the robot can potentially stuck at the classical saddle point (Rimon & Koditschek, 1992). This is a limit case. In fact, in presence of a small perturbation in the y direction, the robot can potentially trace either the continue or the dashed path.

In this work, the idea is to introduce an attractive source \mathbf{x}_a nearby the obstacle, as depicted in Figure 1b. To distinguish the local attractive effect of \mathbf{x}_a from the global one related to the desired position, \mathbf{x}_d is called the “local attractor”, while the name “global attractor” is used to identify \mathbf{x}_d . The local attractor potential field U_a is modelled with the negative exponential function ((Beard & McClain, 2003)):

$$U_a(\mathbf{x}) = -\alpha_a e^{-\frac{\gamma_a}{2}\|\mathbf{x}-\mathbf{x}_a\|^2} \quad (5)$$

where α_a and γ_a are the positive parameters that regulate the intensity and the decay of the attractive effect. In Figure 1b, the circle centred in \mathbf{x}_a identifies the active region U_a^* , defined as the circle with radius R_a^* so that the gradient of U_a goes to zero outside U_a^* . The parameters α_a and γ_a define the active region. For example, U_a^* can be extended all around the obstacle to influence the robot obstacle avoidance on the local attractor side for a good range of approaching directions, i.e. for different \mathbf{x}_s (see the path lines in Figure 1b). Similar to (3), the active region U_a^* is determined by solving $|\nabla U_a| = s_\epsilon$:

$$R_a^* = \left[-\frac{1}{\gamma_a} W_{-1} \left(-\frac{s_\epsilon^2}{\alpha_a^2 \gamma_a} \right) \right]^{1/2} \quad (6)$$

The total potential field with the obstacle and the two attractors becomes:

$$\begin{aligned} U_t(\mathbf{x}) &= U_d(\mathbf{x}) + U_o(\mathbf{x}) + U_a(\mathbf{x}) = \\ &= \frac{1}{2}\sigma\|\mathbf{x}-\mathbf{x}_d\|^2 + \beta_o e^{-\frac{\gamma_o}{2}\|\mathbf{x}-\mathbf{x}_o\|^2} - \alpha_a e^{-\frac{\gamma_a}{2}\|\mathbf{x}-\mathbf{x}_a\|^2} \end{aligned} \quad (7)$$

A generic potential field U_t is shown in Figure 2b. The attractive source \mathbf{x}_a acts bending the potential on its side. For instance, given γ_a , a local minimum may result for high values of the intensity α_a and the robot would stop at the equilibrium point close to \mathbf{x}_a . Anyway, there exist some values of α_a and γ_a for which the total potential field deflates near \mathbf{x}_a without suffering local minima (Figure 3).

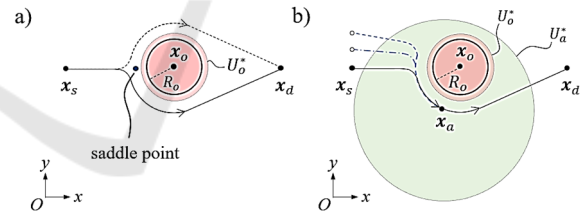


Figure 1: Two-dimensional analysis of the possible robot paths obtained by following the gradient lines of a quadratic potential function, with a single obstacle and a local attractor modelled with the exponential functions. a) In presence of the obstacle, the robot can potentially follow either the dashed or the solid lines; in the same figure, the classical saddle point is shown. b) The robot path is influenced by the local attractor placed on the obstacle side; the styles of the lines identify alternative paths related to different starting positions, i.e. different approaching directions of the robot towards the obstacle.

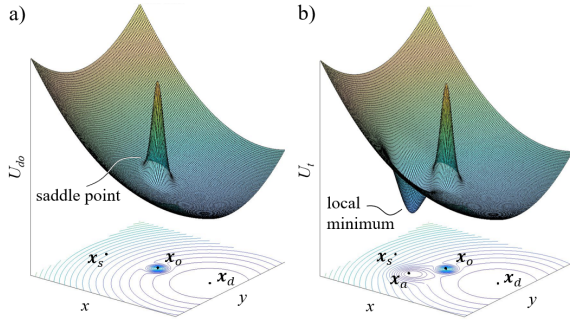


Figure 2: Influence of the exponential repulsive and attractive potential fields on a quadratic potential field; the xy plane, in addition to the significant points, contains the isolines of the potential field. a) Case with a single obstacle; in the same figure, the classical saddle point is shown. b) Case with a single obstacle and a local attractor; the high intensity of the local attractor generates a local minimum, as indicated by the isolines.

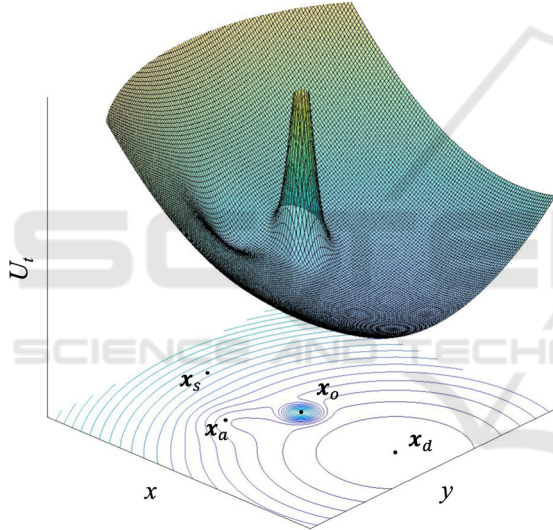


Figure 3: Potential field resulting from a single obstacle and a local attractor. The intensity of the local attractor is limited so that the local minimum does not show, as indicated by the isolines.

2.2 Analysis of the Influence of Local Attractors

When the obstacle is identified, the attractor \mathbf{x}_a can be placed near \mathbf{x}_o to affect the collision avoidance path. It is assumed that \mathbf{x}_a is sufficiently far from the active region U_o^* . Without loss of generality the following relation must hold:

$$\|\mathbf{x}_a - \mathbf{x}_o\| > R_o^* + \tilde{\varepsilon} \quad (8)$$

so that the analysis of the local minimum related to U_a will simplify. The meaning and the lower bound of the positive quantity $\tilde{\varepsilon}$ will be pointed later. Moreover, the following assumption which regulates the size of U_a^* must be satisfied:

$$\|\mathbf{x}_a - \mathbf{x}_d\| \geq R_a^* \quad (9)$$

otherwise, the global minimum would be perturbed. In Figure 4 a generic case which satisfies conditions (8)-(9) is depicted.

To analyse the influence of α_a , the local minimum problem related to \mathbf{x}_a is discussed. This can be dealt by considering the function U_{da} , defined as the sum of the two potential fields of the attractors:

$$U_{da}(\mathbf{x}) = U_d(\mathbf{x}) + U_a(\mathbf{x}) = \frac{1}{2}\sigma\|\mathbf{x} - \mathbf{x}_d\|^2 - \alpha_a e^{-\frac{\gamma_a}{2}\|\mathbf{x} - \mathbf{x}_a\|^2} \quad (10)$$

In fact, because of assumption (8), the local minimum will appear in the region where $U_o \simeq 0$. By studying the points where the gradient vanishes, the condition is:

$$\frac{\partial}{\partial \mathbf{x}} U_{da}(\mathbf{x}) = \sigma(\mathbf{x} - \mathbf{x}_d) + \alpha_a \gamma_a (\mathbf{x} - \mathbf{x}_a) e^{-\frac{\gamma_a}{2}\|\mathbf{x} - \mathbf{x}_a\|^2} = 0 \quad (11)$$

The problem can be further simplified by writing the system (11) in the auxiliary reference frame $O'-x'y'$ with origin in $O' \equiv \mathbf{x}_d$ and whose x' axis is aligned with \mathbf{x}_a (see Figure 4). Thus, by considering $\mathbf{x}'_d = [0 \ 0]^T$ and $\mathbf{x}'_a = [x'_a \ 0]^T$ the system becomes:

$$\frac{\partial}{\partial x'} U_{da}(\mathbf{x}') = \sigma x' + \alpha_a \gamma_a (x' - x'_a) e^{-\frac{\gamma_a}{2}[(x' - x'_a)^2 + y'^2]} = 0 \quad (12)$$

$$\frac{\partial}{\partial y'} U_{da}(\mathbf{x}') = \sigma y' + \alpha_a \gamma_a y' e^{-\frac{\gamma_a}{2}[(x' - x'_a)^2 + y'^2]} = 0 \quad (13)$$

where $\mathbf{x}' = [x' \ y']^T$ is the spatial variable which identifies a point in the auxiliary reference frame. Since σ , α_a and γ_a are positive, (13) is true only for $y' = 0$. This suggests that the local minimum must lie on the x' axis. Therefore, the problem can be studied in one dimension. In fact, by considering $y' = 0$, (12) reduces to:

$$\frac{\partial}{\partial x'} U_{da}(x', 0) = \sigma x' + \alpha_a \gamma_a (x' - x'_a) e^{-\frac{\gamma_a}{2}(x' - x'_a)^2} = 0 \quad (14)$$

Given σ , x'_a and γ_a , equation (14) is parametric in α_a and the number of solutions for x' depend on α_a . This can be visualized by plotting the solution in a

graphical fashion. By considering:

$$A = \sigma x', \quad B = \alpha_a \gamma_a (x' - x'_a) e^{-\frac{\gamma_a}{2}(x' - x'_a)^2} \quad (15)$$

the graphical solution is shown in Figure 5b, for fixed σ , x'_a and γ_a . In Figure 5a, the resulting potential $U_{da}(x', 0)$ is plotted.

For small values of α_a , the curves identifying $-A$ and B have only one intersection point at the global minimum, i.e. in $x' = 0$. By increasing the value of α_a , the potential starts bending around $x' = x'_a$. The value of α_a for which $U_{da}(x', 0)$ shows a saddle point in $x' = \tilde{x}'$, i.e. when the curves $-A$ and B become tangent (dashed line), is then the upper bound $\tilde{\alpha}_a$. For $\alpha_a > \tilde{\alpha}_a$, the green and the blue curves intersect in 3 points, i.e. at the global minimum and at the local stationary points; in this case the local minimum lies in the interval $0 < x' < x'_a$.

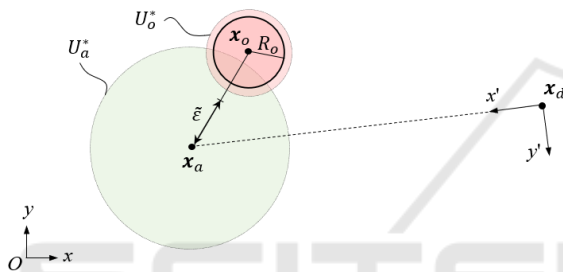


Figure 4: Generic case with the obstacle and the local attractor potential functions designed according to the geometrical constraints.

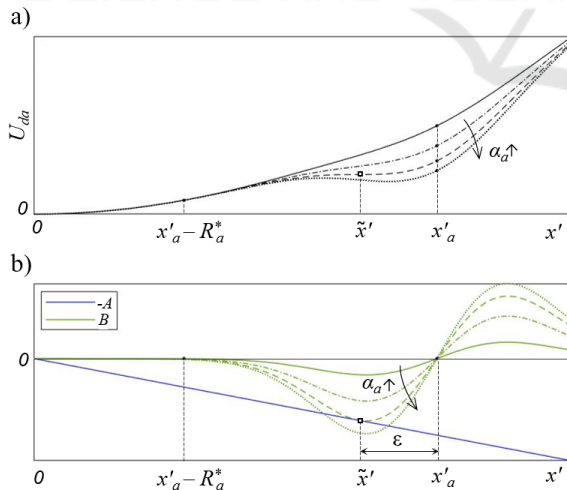


Figure 5: Analysis of the parametric solution of equation (14). The different style of the lines refers to different values of α_a ; the square identify the saddle point related to the local attractor. a) Potential function U_{da} along the x' axis; the saddle point exists for the dashed line, at \tilde{x}' . b) Graphical solution by means of the intermediate variables (15); the saddle point is represented by the point of tangency.

The important result is that, given σ , x'_a and γ_a , if $\alpha_a < \tilde{\alpha}_a$ no local stationary points occur. Hereafter, the saddle point represents the theoretical limit in this sense: the maximum admissible depression near x'_a , i.e. the maximum attraction, is obtained by choosing an α_a just below $\tilde{\alpha}_a$.

Notice that, except where otherwise specified, the saddle point here discussed is the one related to the local attractor; in fact, the one introduced in Figure 1a and Figure 2a has a different meaning and it is identified as the “classical” saddle point.

To find $\tilde{\alpha}_a$, the condition which generates the saddle is studied. In the saddle point, the first and the second derivative must vanish. Therefore, (14) must hold together with the following:

$$\frac{\partial^2}{\partial^2 x'} U_{da}(x', 0) = \sigma + \left[\frac{1}{\gamma_a} - (x' - x'_a)^2 \right] \alpha_a \gamma_a^2 e^{-\frac{\gamma_a}{2}(x' - x'_a)^2} = 0 \quad (16)$$

The system of equations (14) and (16) is verified if (see Appendix B):

$$(\gamma_a)x'^3 - (2x'_a\gamma_a)x'^2 + (x_a'^2\gamma_a)x' - x'_a = 0 \quad (17)$$

which gives the $x' = \tilde{x}'$ where the inflection arises (see Figure 5). The cubic (17) has 3 real solutions for x' if:

$$x'_a > \sqrt{\frac{27}{4\gamma_a}} \quad (18)$$

In this case, the meaningful solution is:

$$\begin{aligned} \tilde{x}'(x'_a, \gamma_a) &= \frac{2}{3}x'_a \left[\cos\left(\frac{\theta + 4\pi}{3}\right) + 1 \right] \\ \theta(x'_a, \gamma_a) &= \cos^{-1}\left(\frac{27}{2\gamma_a x_a'^2} - 1\right) \end{aligned} \quad (19)$$

And by substituting (19) in (14) it results:

$$\tilde{\alpha}_a(\sigma, x'_a, \gamma_a) = \frac{-\sigma \tilde{x}'}{\gamma_a (\tilde{x}' - x'_a) e^{-\frac{\gamma_a}{2}(\tilde{x}' - x'_a)^2}} \quad (20)$$

where it is stressed the dependency of $\tilde{\alpha}_a$ from σ , x'_a and γ_a

In general, even if U_a is centred in x_a , the sum with U_d causes a slight shifting of the inflection in the

direction of the x' axis, in $\tilde{\mathbf{x}}' = [\tilde{x}' \ 0]^T$. The shifting can be quantified considering the distance $\|\mathbf{x}'_a - \tilde{\mathbf{x}}'\| = x'_a - \tilde{x}' = \varepsilon$ (see Figure 5). This aspect has been considered in the assumption (8), so that the saddle point falls outside U_o^* .

In particular, two scenarios can be distinguished. In the first one, the line segment $\mathbf{x}_a\mathbf{x}_d$ does not intersect U_o^* ; in this case, the stationary point would fall outside U_o^* . The second scenario arises if the line segment $\mathbf{x}_a\mathbf{x}_d$ crosses U_o^* : here, if $\|\mathbf{x}_a - \mathbf{x}_o\| \leq R_o^* + \varepsilon$ the saddle point of U_{da} may overlap with the obstacle; thus, when considering the total potential U_t , the saddle may not exist and the control on the attraction effect of \mathbf{x}_a is lost. In this case, the main issue is that the depression which can still manifest within U_a^* would push the robot towards the obstacle, which is not advisable. On the other hand, if $\mathbf{x}_a\mathbf{x}_d$ crosses U_o^* but $\|\mathbf{x}_a - \mathbf{x}_o\| > R_o^* + \varepsilon$, this will not happen.

From this analysis, the value $\tilde{\varepsilon}$ in condition (8) for the two different scenarios is:

$$\begin{aligned} \tilde{\varepsilon} &= 0 && \text{if } \overline{\mathbf{x}_a\mathbf{x}_d} \cap U_o^* = \emptyset \\ \tilde{\varepsilon} &= \varepsilon && \text{if } \overline{\mathbf{x}_a\mathbf{x}_d} \cap U_o^* \neq \emptyset \end{aligned} \quad (21)$$

The steps for sculpting the potential field with local attractors are summarized by the pseudocode in Table 1.

Table 1: Pseudocode of the APF with local attractors.

1. define \mathbf{x}_s and \mathbf{x}_d
2. choose σ
3. identify the obstacle \mathbf{x}_o , R_o
4. choose γ_o, β_o and s_ε
5. use (3) to find R_o^*
6. place the local attractor \mathbf{x}_a outside U_o^*
7. obtain $x'_a = \ \mathbf{x}_a - \mathbf{x}_d\ $, choose γ_a and verify (18)
8. calculate \tilde{a}_a with (20) and choose $a_a < \tilde{a}_a$
9. calculate $\tilde{\varepsilon}$ with (21) and verify (8)
10. find R_a^* with (6) and verify (9)
11. obtain U_t as (7)

In the next section, the influence of local attractors modelled as in Figure 3 is analysed to demonstrate that this principle can be used to drive the robot on the side of the local attractor during the obstacle avoidance manoeuvre, without that the robot get stuck.

3 APPLICATION

The effectiveness of using local attractors is investigated considering the case study of a differential wheeled robot navigating in a structured environment. The gradient tracking method is chosen to take full advantage from the potential field generated with local attractors. This simple and effective technique produces an exact tracking of the gradient lines and can be applied to smooth artificial vector field (Guldner & Utkin, 1995). It consists in regarding the velocity vector rather than the acceleration vector as the variable under control.

The motion is simulated in Gazebo with the Turtlebot[®]. Robot commands are given in terms of linear velocity v and angular velocity ω (Figure 6a).

The angular velocity command is chosen proportional to the angular error φ between the desired direction, identified by the vector \mathbf{v}_d , and the one of the actual velocity \mathbf{v}_r :

$$\omega = K \angle \mathbf{v}_d \mathbf{v}_r = K \varphi \quad (22)$$

where K is the proportional gain and \mathbf{v}_d is chosen as the negative direction of the gradient:

$$\mathbf{v}_d = -\nabla U_t \quad (23)$$

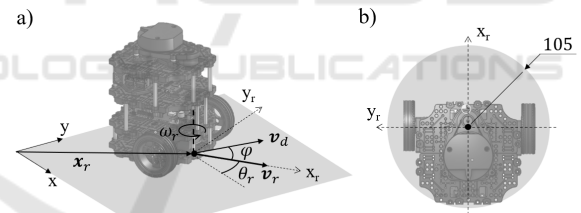


Figure 6: Gradient tracking (a) and robot size (b).

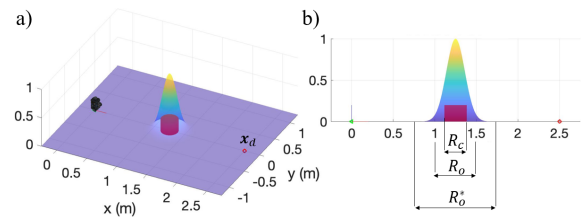


Figure 7: Obstacle potential field. a) three dimensional view; b) lateral view.

As regard the linear velocity command, if $v_r = 0$ at the starting and desired positions, a suitable choice for the linear velocity magnitude is (Guldner & Utkin, 1995):

$$v = \min \left(a_0 t, v_0, (2a_0 d_r(t))^{\frac{1}{2}} \right) \quad (24)$$

where a_0 is the maximum acceleration, v_0 the maximum velocity and $d_r(t) = \|\mathbf{x}_d - \mathbf{x}_r(t)\|$ is the position error.

Different tests are proposed. In each one, a cylindrical obstacle with radius $R_c = 0.135$ m is placed in the middle between the starting and the desired robot positions. To consider the robot size (see Figure 6b), the obstacle potential field is extended to a wider range, as in (Hossain, Habibullah, Islam, & Padilla, 2021). In particular, the parameter γ_o is chosen so that at a distance $R_o = (0.135 + 0.105 + s)$ m the magnitude of the repulsive gradient is 30% of its maximum value, i.e. $|\nabla U_o|_{R_o} = 0.3|\nabla U_o|_{max}$, so its value is set as $\gamma_o = 80.35$. The length s is a safety margin and it is set to 0.01 m. The obstacle and the related potential field obtained with $\beta_o = 1$ are shown in Figure 7, together with the mobile robot in one of its starting positions.

Test 1 is made considering the problem introduced in Figure 1b. The robot starts from different positions $\mathbf{x}_s = [x_s, y_s]^T$ m, with $x_s = 0$ and y_s ranging between 0.05 m and 0.15 m. To influence the robot path regardless of the approaching direction against the obstacle, a local attractor is placed on one side of the obstacle, in $\mathbf{x}_a = [0.64, -0.46]^T$ m. The slight displacement 0.05 m representing the lower limit for y_s is chosen to exclude the limit case discussed in Figure 1a and to let the robot choose the side opposite to \mathbf{x}_a when the local attractor is removed, as will be seen later.

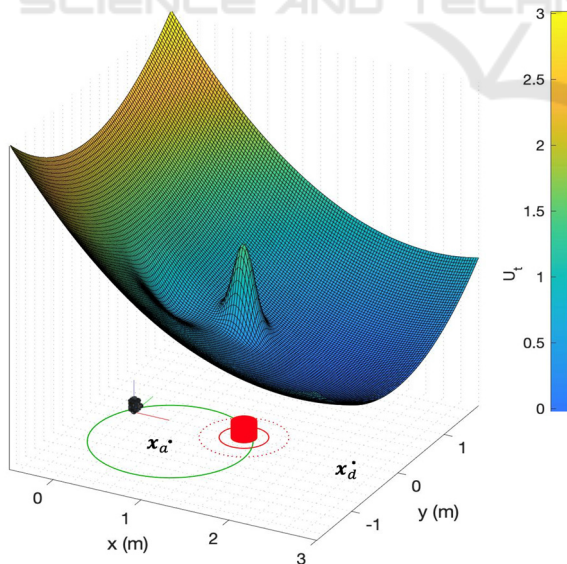


Figure 8: Test layout.

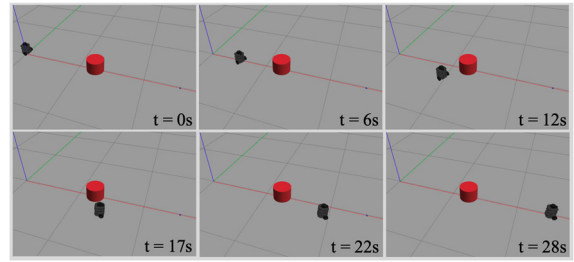


Figure 9: Frames of simulation of Turtlebot in Gazebo.

The global attractor is modelled considering $\mathbf{x}_d = [2.5, 0]^T$ m, $\sigma = 0.5$, while the local attractor potential field is obtained with $\alpha_a = 0.266$ and $\gamma_a = 17.02$. The intensity of the local attractor is chosen as $\alpha_a = 0.8\tilde{\alpha}_a$, where $\tilde{\alpha}_a$ is obtained from (20), given $x'_a = \|\mathbf{x}_a - \mathbf{x}_d\|$.

The layout of test 1 and the potential field U_i are shown in Figure 8. The obstacle position \mathbf{x}_o is known. The gradient of the potential field is computed in Matlab and the commands are sent to the robot through the ROS toolbox, with a control frequency of 30 Hz. The robot motion is characterized by $a_0 = 0.15$ m/s², $v_0 = 0.1$ m/s. and $K = 5$. The robot trajectory is obtained through odometry feedback.

Figure 9 shows the frame of the simulation obtained with $\mathbf{x}_s = [0, 0.05]^T$ m. Results in terms of path are reported in Figure 10a. The robot is attracted by \mathbf{x}_a and avoids the obstacle passing on that side. The effect of the attractor can be seen in Figure 10b, where the gradient lines of U_i are depicted.

To evaluate the effectiveness of the potential field with local attractors, test 2 is performed removing the local attractor, with $\mathbf{x}_s = [0, 0.05]^T$ m. Results are shown in Figure 11a and Figure 11b. The robot follows the gradient and passes the obstacle on the opposite direction, compared to test 1. Moreover, because of the greater curvature of the gradient lines next to the obstacle, the Turtlebot[®] manoeuvre is less smooth.

The last test, identified as test 3, is carried out to analyse the effect of the intensity of the local attractor. Figure 12a shows the different paths obtained with the same starting position $\mathbf{x}_s = [0, 0.05]^T$ m and with different values of α_a . For $\alpha_a = 0.9\tilde{\alpha}_a$, the path curve is sharper near the point $\tilde{\mathbf{x}}$ where the saddle would occur for $\alpha_a = \tilde{\alpha}_a$ (see Figure 12b). This is not recommendable, since regions with high curvature implies sudden change in direction and may saturate the control resources. However, with lower values of α_a the robot can still be guided towards the side of \mathbf{x}_a , as shown by dashed and dotted paths in Figure 12a.

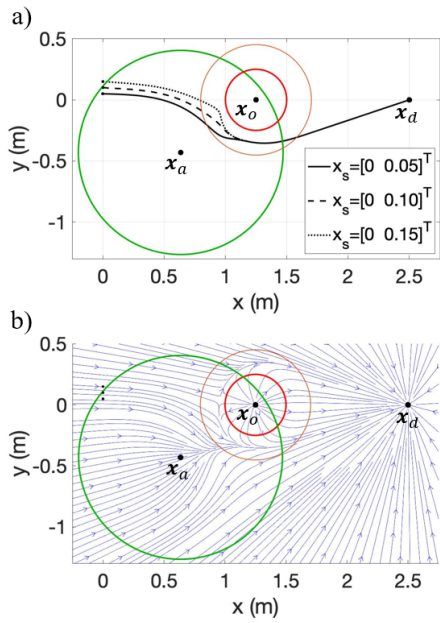


Figure 10: Results of test 1.

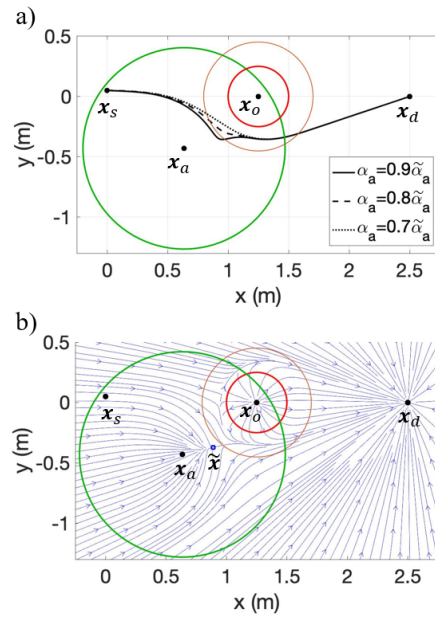


Figure 12: Results of test 3.

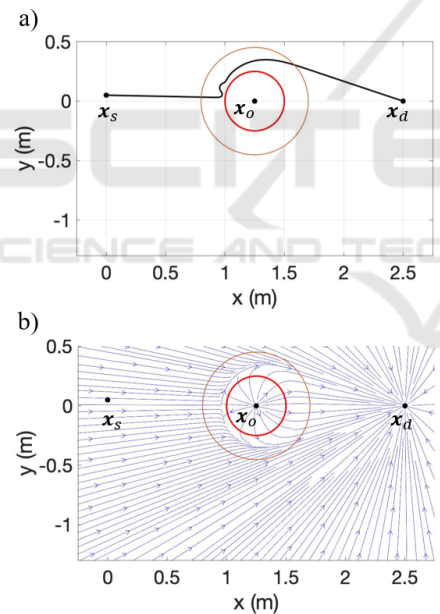


Figure 11: Results of test 2.

4 CONCLUSIONS

A new collision avoidance method which aims to conditionate the robot trajectory by using local attractors has been presented. The method is inspired by the previous studies on artificial potential fields but moves the attention on the role of the attractors rather than the obstacles.

The state of the art of artificial potential fields has been discussed and a lack of works dealing with local attractors have been found. Thus, the idea of a new formula to handle attractors and repulsors coexistence has been developed with the intention to choose preferred directions while avoiding collision.

Section 2 describes the theory. The analysis starts by considering classical exponential functions to model the potential field for the obstacles and the attractors. The intuition has been further investigated by looking for the optimal parameters of the potential functions to generate the maximum deflection in the proximity of a local attractor.

In the result section, the algorithm has been tested on a differential wheeled robot. The robot can avoid the obstacle choosing the local attractor side, even considering different approaching directions. Also, different local attractor intensities have been considered to show how to obtain smooth trajectories by regulating the attractive effect.

Future works will focus on the application to real world scenarios and on the extension to multiple local attractors or multiple obstacles, with the possibility to model the potential field related to the obstacles with different shapes besides disc. Moreover, as the method is based on potential field, it will be interesting to extend the theory with dynamic obstacles and to test how sensory data could affect collision-free trajectories.

REFERENCES

- Abhishek, T. S., Schilberg, D., & Arockia Doss, A. S. (2021). Obstacle Avoidance Algorithms: A Review. *IOP Conference Series: Materials Science and Engineering*, 1012, 012052. <https://doi.org/10.1088/1757-899x/1012/1/012052>
- Arslan, O., & Koditschek, D. E. (2019). Sensor-based reactive navigation in unknown convex sphere worlds. *International Journal of Robotics Research*, 38(2–3), 196–223. <https://doi.org/10.1177/0278364918796267>
- Beard, R., & McClain, T. (2003). Motion planning using potential fields. *Brigham Young University, BYU ScholarsArchive, Faculty Publications 1313*. Retrieved from <http://www.et.byu.edu/~beard/papers/preprints/BeardMcLain03-potential.pdf>
- Castelnovi, M., Sgorbissa, A., & Zaccaria, R. (2006). Ghost-Goal algorithm for reactive safe navigation in outdoor environments. In T. Arai et al. (Eds.) (Ed.), *Intelligent Autonomous Systems 9* (pp. 49–56). IOS Press.
- Chakravorthy, A., & Ghose, D. (1998). Obstacle avoidance in a dynamic environment: A collision cone approach. *IEEE Transactions on Systems, Man, and Cybernetics Part A: Systems and Humans*, 28(5), 562–574. <https://doi.org/10.1109/3468.709600>
- Connolly, C. I., & Grupen, R. A. (1993). The applications of harmonic functions to robotics. *Journal of Robotics Systems*, 10(7), 931–946. <https://doi.org/10.1109/ISIC.1992.225141>
- De Medio, C., & Oriolo, G. (1991). Robot Obstacle Avoidance Using Vortex Fields. *Advances in Robot Kinematics*, 227–235. https://doi.org/10.1007/978-3-7091-4433-6_26
- Filippidis, I., & Kyriakopoulos, K. J. (2011). Adjustable navigation functions for unknown sphere worlds. In *Proceedings of the IEEE Conference on Decision and Control* (pp. 4276–4281). <https://doi.org/10.1109/CDC.2011.6161176>
- Fox, D., Burgard, W., & Thrun, S. (1997). The dynamic window approach to collision avoidance. *IEEE Robotics and Automation Magazine*, 4(1), 23–33. <https://doi.org/10.1109/100.580977>
- Guldner, J., & Utkin, V. I. (1995). Sliding Mode Control for Gradient Tracking and Robot Navigation Using Artificial Potential Fields. *IEEE Transactions on Robotics and Automation*, 11(2), 247–254. <https://doi.org/10.1109/70.370505>
- Guldner, J., & Utkin, V. I. (1996). Tracking the gradient of artificial potential fields: Sliding mode control for mobile robots. *International Journal of Control*, 63(3), 417–432. <https://doi.org/10.1080/00207179608921850>
- Haddadin, S., Urbanek, H., Parusel, S., Burschka, D., Roßmann, J., Albu-Schäffer, A., & Hirzinger, G. (2010). Real-time reactive motion generation based on variable attractor dynamics and shaped velocities. In *IEEE/RSJ 2010 International Conference on Intelligent Robots and Systems* (pp. 3109–3116). Taipei. <https://doi.org/10.1109/IROS.2010.5650246>
- Hossain, T., Habibullah, H., Islam, R., & Padilla, R. V. (2021). Local path planning for autonomous mobile robots by integrating modified dynamic-window approach and improved follow the gap method. *Journal of Field Robotics*, (December), 1–16. <https://doi.org/10.1002/rob.22055>
- Khatib, O. (1986). Real-time obstacle avoidance for manipulators and mobile robots. *International Journal of Robotics Research*, 5(1), 90–98.
- Koppenborg, M., Nickel, P., Naber, B., Lungfiel, A., & Huelke, M. (2017). Effects of movement speed and predictability in human – robot collaboration. *Human Factors and Ergonomics in Manufacturing & Service Industries*, 27(4), 197–209. <https://doi.org/10.1002/hfm.20703>
- LaValle, S. M. (2006). Planning algorithms. *Planning Algorithms*, 9780521862, 1–826. <https://doi.org/10.1017/CBO9780511546877>
- Long, Z. (2020). Virtual target point-based obstacle-avoidance method for manipulator systems in a cluttered environment. *Engineering Optimization*, 52(11), 1957–1973. <https://doi.org/10.1080/0305215X.2019.1681986>
- Mauro, S., Scimmi, L. S., & Pastorelli, S. (2017). Collision avoidance algorithm for collaborative robotics. *International Journal of Automation Technology*, 11(3), 481–489. https://doi.org/10.1007/978-3-319-61276-8_38
- Melchiorre, M., Scimmi, L. S., Mauro, S., & Pastorelli, S. P. (2021). Vision-based control architecture for human–robot hand-over applications. *Asian Journal of Control*, 23(1), 105–117. <https://doi.org/10.1002/asjc.2480>
- Melchiorre, M., Scimmi, L. S., Pastorelli, S. P., & Mauro, S. (2019). Collision Avoidance using Point Cloud Data Fusion from Multiple Depth Sensors: A Practical Approach. *2019 23rd International Conference on Mechatronics Technology, ICMT 2019*. <https://doi.org/10.1109/ICMECT.2019.8932143>
- Murphy, R. R. (2000). *Introduction to AI robotics*. Cambridge, Massachusetts: The MIT Press.
- Paromtchik, I. E., & Nassal, U. M. (1995). Reactive Motion Control for an Omnidirectional Mobile Robot. *Proc. of the Third European Control Conference*, 5–8.
- Pozna, C., Troester, F., Precup, R. E., Tar, J. K., & Preitl, S. (2009). On the design of an obstacle avoiding trajectory: Method and simulation. *Mathematics and Computers in Simulation*, 79(7), 2211–2226. <https://doi.org/10.1016/j.matcom.2008.12.015>
- Qian, K., Ma, X., Dai, X., & Fang, F. (2010). Socially acceptable pre-collision safety strategies for human-compliant navigation of service robots. *Advanced Robotics*, 24(13), 1813–1840. <https://doi.org/10.1163/016918610X527176>
- Ren, J., Mcisaac, K. A., Patel, R. V., & Peters, T. M. (2007). A potential field model using generalized sigmoid functions. *Construction*, 37(2), 477–484.
- Rimon, E., & Koditschek, D. E. (1992). Exact Robot Navigation using Artificial Potential Functions. *IEEE*

Transactions on Robotics and Automation, 8(5), 501–518. <https://doi.org/10.1109/70.163777>

- Scimmi, L. S., Melchiorre, M., Mauro, S., & Pastorelli, S. (2018). Multiple collision avoidance between human limbs and robot links algorithm in collaborative tasks. *ICINCO 2018 - Proceedings of the 15th International Conference on Informatics in Control, Automation and Robotics*, 2, 291–298. <https://doi.org/10.5220/0006852202910298>
- Scimmi, L. S., Melchiorre, M., Mauro, S., & Pastorelli, S. (2019). Experimental Real-Time Setup for Vision Driven Hand-Over with a Collaborative Robot. *2019 International Conference on Control, Automation and Diagnosis, ICCAD 2019 - Proceedings*. <https://doi.org/10.1109/ICCAD46983.2019.9037961>
- Scimmi, L. S., Melchiorre, M., Troise, M., Mauro, S., & Pastorelli, S. (2021). A Practical and Effective Layout for a Safe Human-Robot Collaborative Assembly Task. *Applied Sciences (Switzerland)*, 11(4).
- Siciliano, B., Sciavicco, L., Villani, L., & Oriolo, G. (2009). *Robotics - Modelling, Planning and Control*. *Journal of Chemical Information and Modeling*.
- Volpe, R., & Khosla, P. (1990). Manipulator control with superquadratic artificial potential functions: theory and experiments. *IEEE Transactions on Systems, Man and Cybernetics*, 20(6), 1423–1436.
- Weisstein, E. (2021). Cubic formula. Retrieved June 7, 2021, from <https://mathworld.wolfram.com/CubicFormula.html>
- Zou, X., & Zhu, J. (2003). Virtual local target method for avoiding local minimum in potential field based robot navigation. *Journal of Zhejiang University Science*, 4(3), 264–269.

APPENDIX A

From (2), the gradient of the repulsive potential field is:

$$\begin{aligned} \nabla U_o(\mathbf{x}, \beta_o, \gamma_o) &= \frac{\partial}{\partial \mathbf{x}} U_o(\mathbf{x}, \beta_o, \gamma_o) \\ &= -\beta_o \gamma_o (\mathbf{x} - \mathbf{x}_o) e^{-\frac{\gamma_o}{2} \|\mathbf{x} - \mathbf{x}_o\|^2} \end{aligned} \quad (\text{A1})$$

More precisely, it is written $\nabla U_o(\mathbf{x}, \beta_o, \gamma_o)$ to stress the dependency on β_o and γ_o , that are the design parameters of the potential field related to the obstacle. By considering $r_o = \|\mathbf{x} - \mathbf{x}_o\|$, the modulus of the gradient can be written as:

$$|\nabla U_o|(r_o, \beta_o, \gamma_o) = \beta_o \gamma_o r_o e^{-\frac{\gamma_o}{2} r_o^2} \quad (\text{A2})$$

Outside of the active region the gradient goes to zero. To quantify this condition, it is assumed that the gradient magnitude is less than or equal to a small value s_ϵ . Thus, by placing $|\nabla U_o|(r_o, \beta_o, \gamma_o) = s_\epsilon$ in (A2) and by taking the square, the following relation holds:

$$-\gamma_o r_o^2 e^{-\gamma_o r_o^2} = -\frac{s_\epsilon^2}{\beta_o^2 \gamma_o} \quad (\text{A3})$$

which can be written as:

$$\begin{aligned} w e^w &= u_\epsilon \\ w &= -\gamma_o r_o^2, \quad u_\epsilon = -\frac{s_\epsilon^2}{\beta_o^2 \gamma_o} \end{aligned} \quad (\text{A4})$$

Equation (A4) can be solved with the Lambert W function as long as $s_\epsilon^2 \leq \beta_o^2 \gamma_o / e$. Since the latter condition is easily verified in practice, (A4) has two real solutions. Without loss of generality, the meaningful solution corresponds to the lower branch W_{-1} :

$$w = W_{-1}(u_\epsilon) \quad (\text{A5})$$

Equation (A5) solved for r_o gives (3).

APPENDIX B

From (14):

$$\alpha_a \gamma_a e^{-\frac{\gamma_a}{2} (x' - x'_a)^2} = \frac{-\sigma x'}{(x' - x'_a)} \quad (\text{B1})$$

By recognizing this term in (16) and substituting, it results the cubic (17), which can be written as:

$$x'^3 - (2x'_a)x'^2 + (x_a'^2)x' - \frac{x'_a}{\gamma_a} = 0 \quad (\text{B2})$$

Equation (B2) can be solved using the cubic formula (Weisstein, 2021). By considering $b_2 = 2x'_a$, $b_1 = x_a'^2$ and $b_0 = -x'_a/\gamma_a$, the cubic has three real solutions if the polynomial discriminant D is negative:

$$D = Q^3 + P^2 = x_a'^2 \left(\frac{1}{4\gamma_a} - \frac{x_a'^2}{27} \right) < 0 \quad (\text{B3})$$

$$\begin{aligned} Q &= \frac{3b_1 - b_2^2}{9} = -\frac{x_a'^2}{9} \\ P &= \frac{9b_2b_1 - 27b_0 - 2b_2^3}{54} = -\frac{x_a'^3}{27} + \frac{x'_a}{2\gamma_a} \end{aligned}$$

Since x'_a is positive, condition (B3) translates into (18). In this case, the three solutions are:

$$\begin{aligned} x'_I &= 2\sqrt{-Q} \cos\left(\frac{\theta}{3}\right) - \frac{b_2}{3} \\ x'_{II} &= 2\sqrt{-Q} \cos\left(\frac{\theta + 2\pi}{3}\right) - \frac{b_2}{3} \\ x'_{III} &= \tilde{x}' = 2\sqrt{-Q} \cos\left(\frac{\theta + 4\pi}{3}\right) - \frac{b_2}{3} \\ \theta &= \cos^{-1}\left(\frac{P}{\sqrt{-Q^3}}\right) \end{aligned} \quad (\text{B4})$$

By substituting the three roots in (14), as many values for α_a can be found.

Figure B1 shows the meaning of the three solutions of a generic case, given σ , x'_a and γ_a . The first root x'_I , represented by the dashed curve, gives a negative α_a . The dotted curve refers to the root x'_{II} and to a high positive value of α_a , which gives the tangency nearby the global minimum still producing a local minimum around x'_a . The only meaningful solution for the case study of this paper is then x'_{III} , which can be written in the form (19).

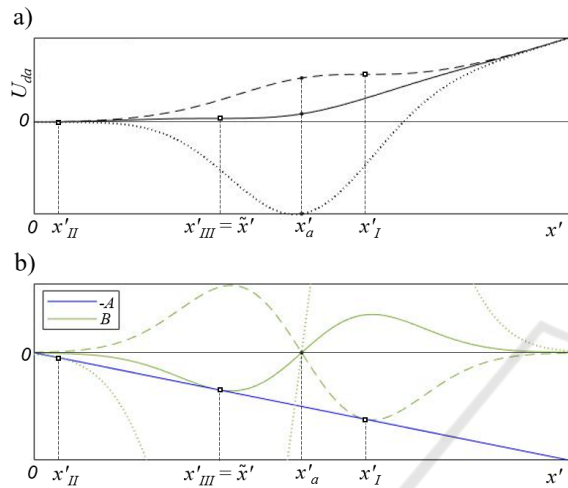


Figure B1: Analysis of the parametric solution of equation (14). The different style of the lines refers to the 3 values of α_a obtained with x_I , x_{II} and x_{III} . a) Potential function U_{da} along the x' axis. b) Graphical solution by means of the intermediate variables (15); the squares identify the points of tangency.